J. of Supercritical Fluids 81 (2013) 254–264

Contents lists available at ScienceDirect

The Journal of Supercritical Fluids

journal homepage: www.elsevier.com/locate/supflu

Frequency response of microcantilevers immersed in gaseous, liquid, and supercritical carbon dioxide

Erdal Uzunlar[a,1], Burcu Beykal[a], Katjana Ehrlich[b,2], Deniz Sanli[a], Alexandr Jonáš[b], B. Erdem Alaca[c], Alper Kiraz[b,e], Hakan Urey[d], Can Erkey[a,e,*]

[a] Department of Chemical and Biological Engineering, Koc University, Istanbul, 34450, Turkey
[b] Department of Physics, Koc University, Istanbul, 34450, Turkey
[c] Department of Mechanical Engineering, Koc University, Istanbul, 34450, Turkey
[d] Department of Electrical and Electronics Engineering, Koc University, Istanbul, 34450, Turkey
[e] Koç University TÜPRAŞ Energy Center (KUTEM), Koç University, 34450 Sarıyer, Istanbul, Turkey

ARTICLE INFO

Article history:
Received 25 February 2013
Received in revised form 27 June 2013
Accepted 28 June 2013

Keywords:
Microcantilevers
Resonant frequency
Quality factor
Carbon Dioxide
Supercritical Fluid

ABSTRACT

The frequency response of ferromagnetic nickel microcantilevers with lengths ranging between 200 μm and 400 μm immersed in gaseous, liquid and supercritical carbon dioxide (CO_2) was investigated. The resonant frequency and the quality factor of the cantilever oscillations in CO_2 were measured for each cantilever length in the temperature range between 298 K and 323 K and the pressure range between 0.1 MPa and 20.7 MPa. At a constant temperature, both the resonant frequency and the quality factor were found to decrease with increasing pressure as a result of the increasing CO_2 density and viscosity. Very good agreement was found between the measured cantilever resonant frequencies and predictions of a model based on simplified hydrodynamic function of a cantilever oscillating harmonically in a viscous fluid valid for Reynolds numbers in the range of [1;1000] (average deviation of 2.40%). At high pressures of CO_2, the experimental *Q*-factors agreed well with the predicted ones. At low CO_2 pressures, additional internal mechanisms of the cantilever oscillation damping caused lowering of the measured *Q*-factor with respect to the hydrodynamic model predictions.

1. Introduction

Microcantilevers have been studied extensively in recent years because of their potential for highly sensitive and low cost compact device applications which include biological and chemical sensors [1–5], viscometers and densitometers [6–14], devices for mechanical characterization of solids [15], and analysis of thermal forces in rarefied gases [16]. In a typical application, microcantilevers are oscillated using either external driving or thermal forces and observed changes in their frequency response are linked to the experimental quantity of interest. The frequency response of an oscillating microcantilever can be characterized by its resonant frequency, ω_R, and the quality factor of the oscillations, *Q*-factor [3]. ω_R is defined as the angular frequency at which the maximum amplitude of oscillation is observed. *Q*-factor quantifies energy dissipation during oscillation; it is a dimensionless parameter defined as the ratio of ω_R to the bandwidth of the cantilever resonance peak. A smaller resonance bandwidth implies a higher *Q*-factor and, thus, lower losses. When an oscillating cantilever is immersed in a fluid of finite density and viscosity, the fluid surrounding the cantilever becomes set in motion. This moving fluid exerts hydrodynamic forces on the cantilever which in turn change the dynamics of cantilever oscillations. In general, these fluid forces can be divided into an inertial part associated with an effective added mass due to the density of the fluid moving along with the cantilever, and a dissipative part describing energy loss due to viscous drag in the fluid [17]. The action of the hydrodynamic forces then leads to a change in the values of ω_R and *Q*-factor observed in the fluid with respect to their vacuum values.

Oscillatory motion of a solid elastic body immersed in a viscous fluid has been subjected to numerous theoretical and experimental studies [4–14]. Currently, there exist two main approaches for the theoretical treatment of the problem. In the simpler one, changes of the shape of an oscillating elastic cantilever is neglected, and the cantilever is modeled as a rigid body moving through the fluid in an external harmonic potential which represents the elastic bending force [11,18,19]. Essentially, the cantilever is treated as a simple damped harmonic oscillator with an effective geometric mass and

* Corresponding author at: Department of Chemical and Biological Engineering, Koc University, Istanbul, 34450 Turkey. Tel.: +90 212 338 1866.
E-mail address: cerkey@ku.edu.tr (C. Erkey).
[1] School of Chemical and Biomolecular Engineering, Georgia Institute of Technology, Atlanta, GA 30332-0100, USA.
[2] Institute of Physics and Astronomy, University of Potsdam, Karl-Liebknecht-Strasse 24-25, 14476 Potsdam, Germany.

0896-8446/$ – see front matter © 2013 Elsevier B.V. All rights reserved.
http://dx.doi.org/10.1016/j.supflu.2013.06.013

viscous damping coefficient depending on the fluid density and viscosity and the frequency of oscillations [17]. Oden et al. adopted this model to monitor viscosity changes in glycerol/water mixtures of various concentrations [11]. A study by McLoughlin et al. [18] provided a method for determining the density and viscosity of an unknown fluid using reference measurements in air and two additional fluids with known properties. Ma et al. analyzed thermal fluctuations of immersed cantilevers to study the microrheological behavior of fluids near a solid/liquid interface [19].

A more rigorous approach to the modeling of the frequency response of immersed cantilevers is based on solving the equation of motion for a clamped elastic beam subject to hydrodynamic forces of the surrounding fluid. This approach was first introduced by Sader [20] who studied the resonant frequency and the *Q*-factor of immersed cantilevers with arbitrary cross section and expressed these quantities as transcendent functions of the density and viscosity of the ambient fluid. A similar approach was later followed by other authors [7,10,14]. The theoretical results derived by Sader [20] were experimentally validated by two studies of Sader et al. using single-crystal silicon AFM microcantilevers immersed in different gases and liquids [6,13], and a good agreement with the calculations was found. These studies [6,13] also described procedures for calibrating the geometric and elastic parameters of the cantilevers by reference measurements in fluids of known properties. Schilowitz et al. developed a similar model in which the fluid viscosity could be directly calculated from the measured viscous damping coefficient of the cantilever [14]. Maali et al. [21] derived an analytical approximation to the complex hydrodynamic function of Sader [20], which was then used by Youssry et al. to obtain closed formulas for the fluid density and viscosity [7]. In that work, the fluid density and viscosity were calculated from the measured resonant frequency and *Q*-factor and known geometry and density of the cantilever. Recently, Papi et al. showed equivalence of the two modeling approaches (simple harmonic oscillator and oscillating elastic beam immersed in a fluid) within the validity range of Maali's approximation to the cantilever hydrodynamic function [12]. Using Maali's formalism, Toda et al. [22] investigated the phase transition between gaseous CO_2 and supercritical CO_2 at 313 K and pressures up to 11.6 MPa with silicon (Si) microcantilevers. According to their study, a significant reduction of the resonant frequency could be detected in the region close to the phase transition.

Since all the models of motion of immersed cantilevers that are utilized in fluid characterization are based on simplifying assumptions (in particular, small dissipation, weak coupling of individual oscillation modes, and cantilever length greatly exceeding its width), it is necessary to evaluate their validity for each specific studied experimental situation. For this purpose, reliable experimental techniques capable of operating under a wide range of ambient conditions need to be developed. In the context of model validation, it is particularly interesting to work with fluids near their critical point and examine the dynamics of the immersed cantilever oscillations in different phases of the fluid (liquid, gaseous, and supercritical fluid). The thermophysical properties of fluids such as density and viscosity can be systematically altered by changing the fluid pressure and temperature. In the proximity of the critical point, small changes in temperature and pressure will have a great impact on the fluid density and viscosity. Hence, near-critical and supercritical fluids represent a challenging system for the experimental characterization of immersed microcantilevers and theoretical modeling of their response.

In this study, we investigate the frequency response of microcantilevers immersed in gaseous, liquid, and supercritical carbon dioxide (CO_2) under a wide range of pressures and temperatures below and above the critical point. We have chosen CO_2 as the model fluid since its critical temperature of 304 K and the pressure of 7.38 MPa can be readily accessed. Supercritical CO_2 ($scCO_2$) is also technologically important as a solvent for a wide range of applications [23–25]. Moreover, the density, viscosity, and other thermophysical properties of CO_2 in different fluid phases are known with high accuracy [26].

First, we describe the fabrication process of nickel-made ferromagnetic microcantilevers. Then, we introduce our experimental setup based on a high-pressure vessel with the control of the pressure and temperature of its contents, magnetic actuation of the cantilever oscillations, and optical readout of the cantilever displacement. We also describe the measurement procedure which consists of driving the cantilevers with AC magnetic field of varying frequency and measuring the amplitude and phase of their frequency response. Subsequently, we present our experimental data acquired using cantilevers of varying length immersed in CO_2 within a wide range of pressures and temperatures. Finally, we compare the frequency response data obtained in different CO_2 phases to the predictions of a frequency response model based on a simplified hydrodynamic function of a cantilever oscillating harmonically in a viscous fluid. We show a very good agreement between the experiments and the model, thus illustrating suitability of our experimental approach for density and viscosity measurements in near-critical and supercritical fluids and characterization of phase transitions in such fluid systems.

2. Materials and methods

2.1. Fabrication of cantilevers

Ferromagnetic microcantilevers made of nickel were produced using established microfabrication methods previously reported by Ozturk et al. [27]. The flow chart of the cantilever fabrication process and a micrograph of a resulting cantilever with a length of 250 μm are shown in Fig. 1.

First, ⟨1 0 0⟩ Si wafers with a diameter of 4 inches, a thickness of 525 ± 25 μm, and a resistivity of 0.1–0.5 Ω cm were cleaned using acetone, isopropyl alcohol, and deionized water and blow-dried with N_2 (Fig. 1a (i)). By using RF-magnetron sputtering, an adhesion-promoting Cr layer of 10–20 nm thickness (Fig. 1a (ii)) and an Au layer of 100–120 nm thickness (Fig. 1a (iii)) were deposited on Si. A film of photoresist (PR) AZ 5214E was spin-coated over the seed layer (Fig. 1a (iv)) and patterned (Fig. 1a (v)).

After patterning, the wafer was sliced into 1 cm × 1 cm dice and the cantilever structural layer was formed via Ni electroplating over the Au surface in a nickel sulphamate bath (Fig. 1a (vi)). Ni was used as the structural layer due to its high resistance to oxidative and corrosive agents, and its ferromagnetic behavior, i.e. the ability to be magnetically actuated. On the basis of the results of Luo et al. [28], the temperature during electroplating was kept constant at 318 K in order to achieve the highest modulus of elasticity. The current density was held constant at 10 mA/cm^2, in order to eliminate internal stress gradient along the length of the cantilever which could possibly cause cantilever stiction to the substrate after release. A 0.85–0.95 μm thick Ni electrodeposition was achieved over a period of 25 min.

After the photoresist removal (Fig. 1a (vii)), Au seed layer was etched for 60–70 s using 1:3 Transene TFAC Ni-selective Au etchant-water solution (Fig. 1a (viii)). Then, Cr layer was etched for 30–45 s using 1:3 MicroChrome TFE Cr etchant-water solution (Fig. 1a (ix)). Over a range of experiments, it has been validated that wider and longer microcantilevers can be produced only by preserving the Au and Cr layers underneath the Ni layer [29]. Thus, timing of each etching step was adjusted so that the Au and Cr layers were only removed outside of the cantilevers.

In the final step, the cantilevers were completely released by anisotropic etching of Si substrate using 45% KOH—water solution

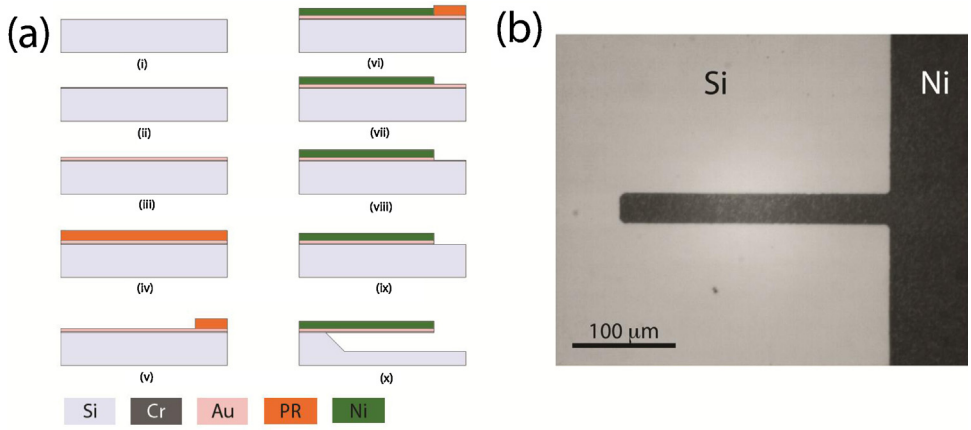

Fig. 1. (a) Flow chart of the fabrication process of nickel (Ni) microcantilevers (see explanation of individual steps in the text). (b) Micrograph of a 250 μm-long Ni cantilever.

at 328 K for 23 h resulting in an etch depth of 150 μm (Fig. 1a (x)) which is the height difference between the Ni anchor and Si base. The depth of 150 μm is sufficient to eliminate the squeezed film damping effects influencing the dynamics of the cantilever oscillations [30]. The temperature and concentration of KOH for Si etching were optimized to overcome the stiction problem. In this study, cantilevers with a width of 20 μm, a thickness of about 1 μm, and lengths of 200 μm, 225 μm, 325 μm and 400 μm were obtained without any stiction to the Si substrate.

2.2. Experimental setup and procedures for measuring the cantilever frequency response

Frequency responses of microcantilevers immersed in various fluid phases of CO_2 were characterized using a home-made experimental setup which was built around a high-pressure sample chamber (see Figs. 2 and 3). Before the measurements, a die with microcantilevers and an electromagnetic actuator – a coil made from Cu wire – were firmly attached to a custom-made Teflon housing (Fig. 3b). The Teflon housing holding the die and the driving coil was then placed into the cylindrical sample chamber, a 50 ml TharSFC 05424-4 high-pressure vessel with sapphire view windows at each face (Fig. 3a). The electrical connection for the actuation of microcantilevers in the pressure vessel was achieved using insulated CONAX Technologies TG24 T gland assemblies that were leak-proof in the studied pressure range (up to ~21 MPa). Subsequently, the vessel was filled with pure CO_2 (Linde, indicated purity of 99.995% by volume) using a TELEDYNE ISCO D Series syringe pump (Fig. 3c). The cantilevers were completely immersed in the ambient fluid, and they were free to move without any observable surface stiction or fluid streaming effects. In order to control the temperature of the fluid in the vessel, plastic tubing was wrapped around the vessel (Fig. 3a) and connected to a water circulator with a constant-temperature heat bath (PolyScience). The temperature and the pressure within the vessel were continuously monitored using a thermocouple with an accuracy of ±1 K and a pressure transducer, respectively (both Omega Engineering Inc). The temperature and the pressure ratings of the vessel were 423 K and 41.4 MPa, respectively.

During the experiments, the die with the microcantilevers mounted inside the vessel could be imaged through the window at the vessel front face using an objective lens with 50 mm focal length, LED-based epi-illumination system (not shown in Fig. 2), and a CCD camera. The ferromagnetic nickel cantilevers were magnetically actuated via the coil that was driven by a sinusoidal signal generated by a function generator (Agilent 33220A) and amplified 50× by a high-voltage, high-frequency amplifier (Falco Systems WMA-300). The frequency and amplitude of the driving sinusoidal signal were computer-controlled using Instrument Control Toolbox in Matlab. The deflections of the driven cantilevers were then recorded using a custom made setup based on optical readout analogical to the standard AFM detection scheme. A near-infrared laser beam (wavelength 780 nm, maximal power 4.5 mW, CPS 192, Thorlabs) was first transformed with a telescope consisting of two identical lenses (f = 30 mm) and then focused on the cantilever with the same objective that was used for cantilever imaging. Laser light back-reflected from the cantilever was collected by the objective and then focused on a quadrant photodiode (QPD) that could register the position of the incident light spot within its surface. Due to cantilever deflections, the angle of reflection of the laser beam from the cantilever changed which subsequently led to changes in the position of the laser spot on the QPD; this provided the cantilever deflection signal. Adjustment of the separation distance between the lenses of the beam transformation telescope allowed moving the focal plane of the laser beam with respect to the objective imaging plane, thus optimizing the deflection signal. In order to select a specific microcantilever for the measurement, the pressure vessel was mounted on an x–y–z translation stage that allowed precise positioning of the cantilevers with respect to the focus of the detection laser beam. The adjustment of the focal spot position was done visually by observing both the cantilever and the laser spot by the CCD camera. In order to improve the signal-to-noise ratio in the cantilever deflection measurements, a phase-sensitive detection scheme was implemented. To this end, the output signal from the QPD was fed into a lock-in amplifier (SR530, Stanford Research Systems) the reference input of which was connected to the function generator driving the cantilevers. With this arrangement, it was possible to detect both the amplitude of the cantilever deflection and its phase shift with respect to driving at a given driving frequency. Both amplitude and phase outputs of the lock-in amplifier were digitalized using a data acquisition board (PCIe-6363, National Instruments) and the same Matlab routine that also controlled the function generator parameters. In a typical experiment, the cantilever driving frequency was swept over a range of 8 kHz roughly centered on the manually found cantilever resonant frequency, and the cantilever response was measured at 400 discrete frequencies distributed uniformly within the sweep range. The amplitude of the driving sinusoidal signal at the output of the function generator was set to 2 V peak-to-peak for measurements in the gaseous and supercritical CO_2 phases, and 3 V peak-to-peak for measurements in the liquid CO_2 phase. Higher amplitude of the driving signal used in the liquid CO_2 measurements compensated weaker deflection signal recorded from cantilevers oscillating in the liquid. Thus, the signal-to-noise ratio of

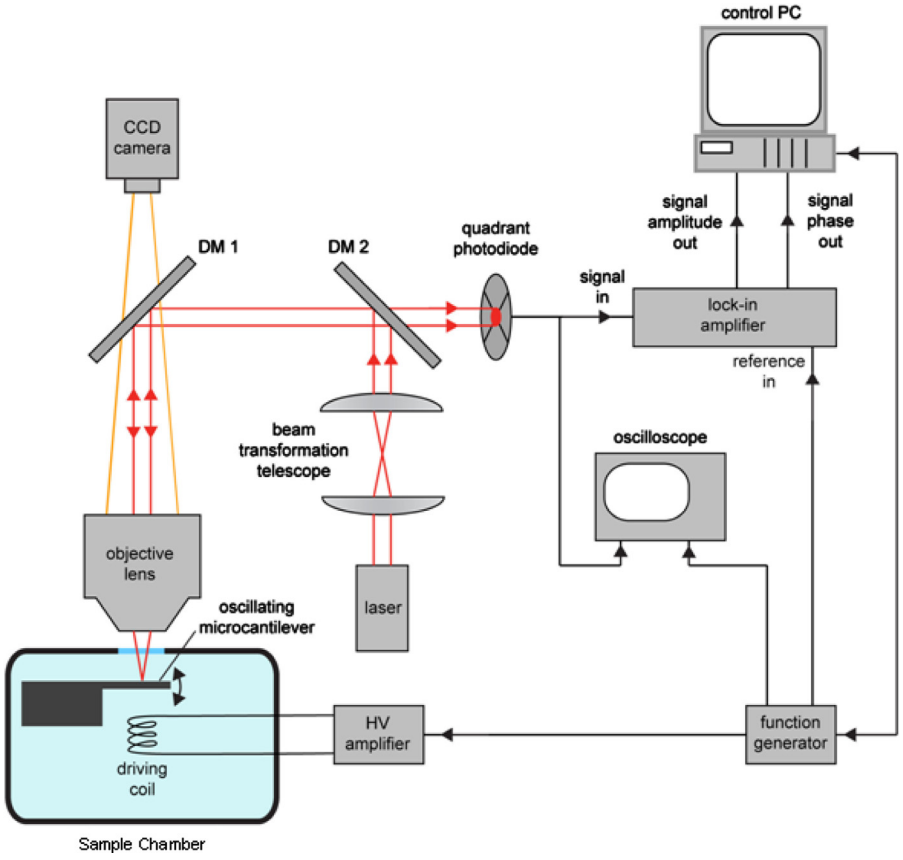

Fig. 2. Schematics of the experimental setup for characterizing the frequency response of immersed microcantilevers. DM1, DM2–dichroic mirrors.

the measurements was kept approximately constant in all studied phases of CO_2.

Systematic mapping of the cantilever frequency response under varying pressure and temperature of the fluid was carried out as follows. First, we filled the sample chamber with CO_2 to the maximal working pressure ranging between 17.23 MPa and 20.68 MPa, and then brought the contents of the sample chamber to the desired temperature. After temperature equilibration (typically 1–2 h), we started the measurements at the highest fluid pressure, and then gradually decreased the pressure down to the atmospheric level, recording data at intermediate pressure levels and a constant temperature. At each studied pressure and temperature level, we recorded the frequency responses of cantilevers of different lengths. We performed three repeated measurements with each cantilever in order to quantify the reproducibility of the obtained cantilever resonant parameters. Since the mechanical properties and exact dimensions of each individual cantilever with the same nominal length slightly varied, we used the same cantilevers in measurements done at all studied temperatures.

According to Sader, the frequency response $A(\omega)$ of an immersed oscillating elastic cantilever in the limit of small dissipation (i.e. high Q) can be approximated by the frequency response of a simple damped harmonic oscillator [13,20]:

$$A(\omega) = \frac{A_0\,\omega_{fluid}^2}{\sqrt{\left(\omega^2 - \omega_{fluid}^2\right)^2 + \frac{\omega^2\,\omega_{fluid}^2}{Q^2}}}. \quad (1)$$

Here, $\omega = 2\pi f$ is the angular driving frequency, A_0 is the zero-frequency amplitude of the response, Q is the quality factor, and $\omega_{fluid} = 2\pi f_{fluid}$ corresponds to the resonant frequency of the cantilever in the fluid in the absence of dissipation. ω_{fluid} is then related to the actual resonant frequency of the damped cantilever in the fluid ω_R (i.e. the frequency of the maximal measured amplitude of the cantilever oscillations) by:

$$\omega_{fluid} = \frac{\omega_R}{\sqrt{1 - \frac{1}{2Q^2}}} \quad (2)$$

Using the above formalism, we fitted the measured frequency responses with Eq. (1), employing nonlinear curve fitting implemented in Matlab. An example of experimental data together with the corresponding fit for data #3 can be seen in Fig. 4. For the other data sets similar fits are obtained. In this figure, three consecutive measurements are shown which were carried out using a 200 μm-long cantilever in gaseous CO_2 at 298 K and 5.63 MPa. A very good agreement of the experimental data with the model given by Eq. (1) is evident. Resonant frequencies f_{fluid} determined from the consecutive measurements are 17632 Hz, 17692 Hz, and 17622 Hz. The mean resonant frequency and the standard deviation for this sample set are 17649 Hz and 38 Hz, respectively, which translates to a relative uncertainty of $\sim 2 \times 10^{-3}$ in resonant frequency. Similar standard deviations of the cantilever resonant frequency were observed in the measurements carried out with all studied cantilever lengths at different temperatures and pressures. The corresponding values of the Q-factor for the frequency responses shown in Fig. 4 are 17.6, 18.2, and 19.6, with the mean value of 18.5 and the standard deviation of 1.03. A higher relative error in measuring the Q-factor in comparison to the measurement of f_{fluid} was a general trend observed for all studied cantilever lengths. However, the typical relative error of the Q-factor measurement remained below 10% throughout all measurements.

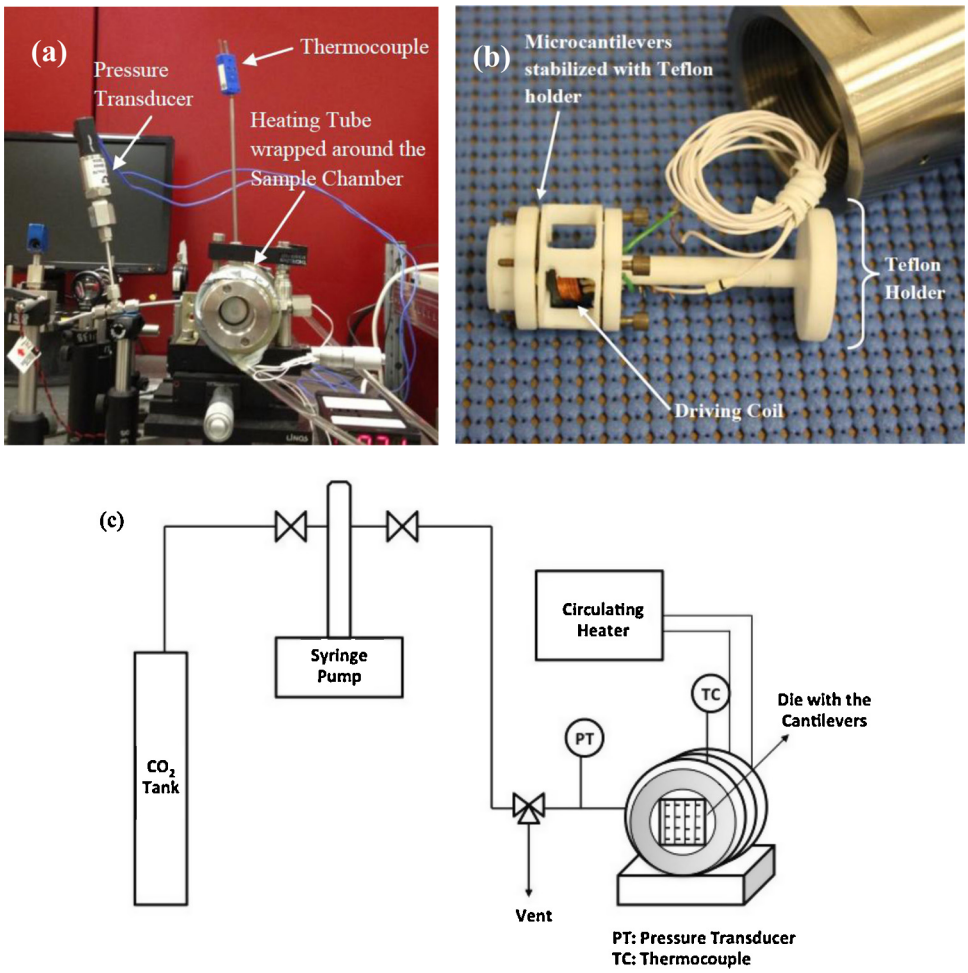

Fig. 3. (a) High-pressure sample chamber mounted on an *x*–*y*–*z* translation stage with attached pressure transducer, thermocouple, and heating tubing. (b) Detail of Teflon holder bearing the die with microcantilevers and the driving coil. (c) Schematics of the system for the sample chamber pressurization.

3. Results and discussion

The results of mapping of the cantilever frequency response in various fluid phases of CO_2 are summarized in Figs. 5–8. In each of these figures, measured resonant frequencies f_{fluid} and *Q*-factors are presented for cantilevers of different lengths at a constant temperature and varying fluid pressure. At the lowest studied temperature of 298 K, phase transition from the gaseous to the liquid phase of CO_2 occurs at the pressure of 6.43 MPa while at the remaining studied temperatures (308 K to 328 K), state of CO_2 changes from gaseous to supercritical upon crossing the critical pressure of 7.38 MPa [26].

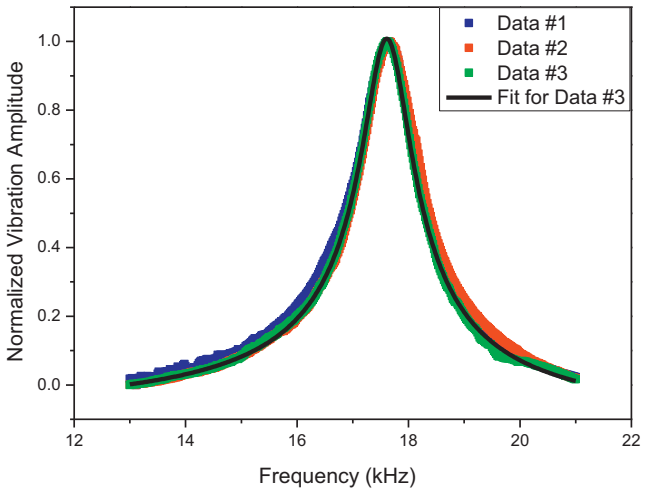

Fig. 4. An example of experimentally measured cantilever frequency response. The three shown sets of data correspond to three consecutive measurements carried out with a 200 μm-long cantilever in gaseous CO_2 at 298 K and 5.63 MPa.

Changes in CO_2 pressure at a constant temperature are accompanied by corresponding changes in the fluid density and viscosity which become pronounced especially in the proximity of the phase transition point. In particular, both density and viscosity of CO_2 increase with increasing fluid pressure [26]. As argued in the introduction, presence of the fluid changes the resonant properties of an immersed cantilever due to the effects of an additional fluid mass moving along with the cantilever and viscous damping of the cantilever motion. Increase in added mass which causes lowering of the cantilever resonant frequency f_{fluid} is mainly associated with the higher fluid density at higher pressure. However, increasing viscosity also plays a role in the inertial effects of the fluid since viscosity determines the effective distance over which the fluid is affected by the cantilever motion and, thus, the effective volume of the fluid moving with the cantilever; this volume increases with increasing viscosity. Correspondingly, higher viscous damping due to the increase of the fluid viscosity with pressure leads to broadening of the cantilever frequency response. In combination with the simultaneous decrease of f_{fluid}, this lowers the value of the *Q*-factor at higher pressure. These semi-quantitative arguments can be used for explaining the trends observed in Figs. 5–8.

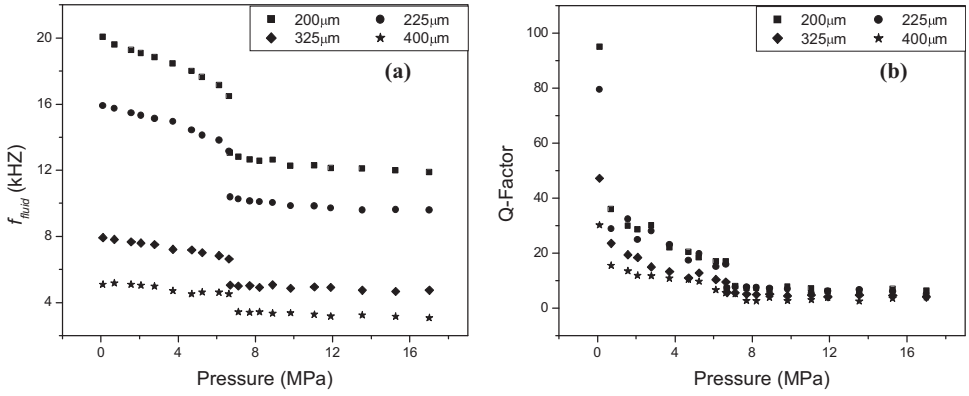

Fig. 5. Variation of (a) f_{fluid} and (b) Q-factor with pressure at 298 K for different cantilever lengths.

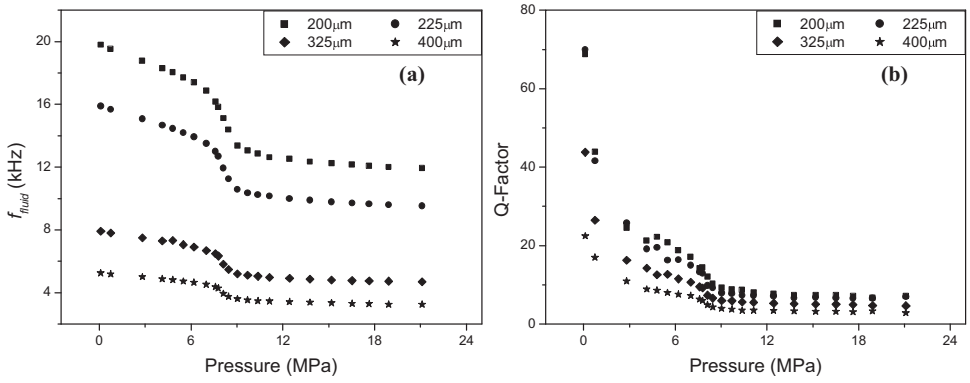

Fig. 6. Variation of (a) f_{fluid} and (b) Q-factor with pressure at 308 K for different cantilever lengths.

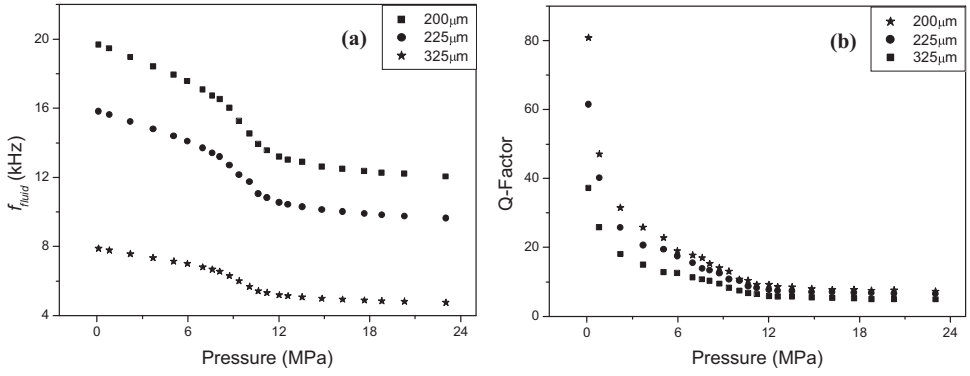

Fig. 7. Variation of (a) f_{fluid} and (b) Q-factor with pressure at 318 K for different cantilever lengths.

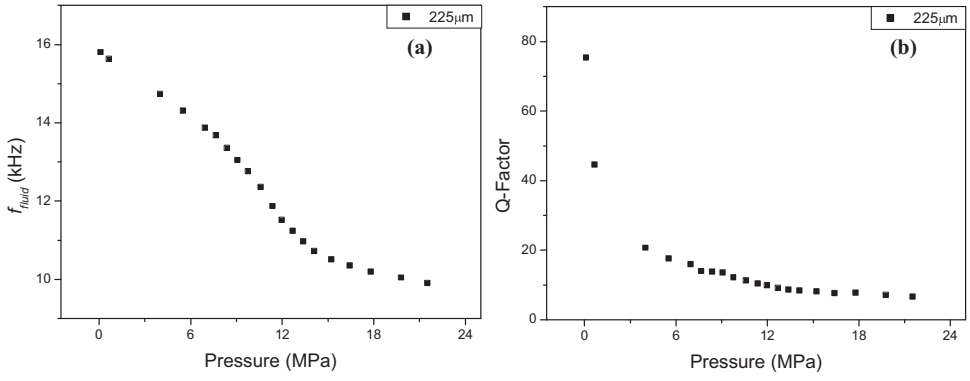

Fig. 8. Variation of (a) f_{fluid} and (b) Q-factor with pressure at 328 K.

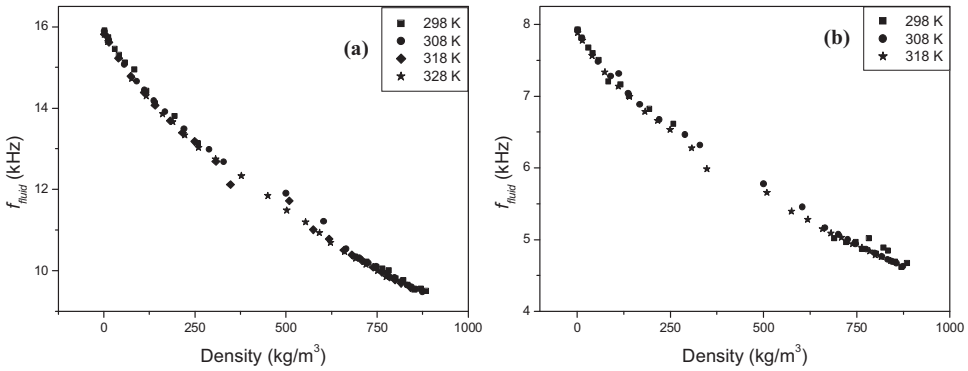

Fig. 9. Variation of f_{fluid} with density for (a) 225 μm cantilevers and for (b) 325 μm cantilevers.

For all studied temperatures and cantilever lengths, measured resonant frequency f_{fluid} increases monotonously with decreasing pressure which correlates with the decreasing fluid density and viscosity. The slope of the dependence of f_{fluid} on the fluid pressure is higher for shorter cantilevers at any given pressure, thus implicating higher sensitivity of the response of such shorter cantilevers to the changing fluid parameters. The discontinuity in f_{fluid} at 298 K indicates the phase change of CO_2 from liquid to gas when the pressure of 6.43 MPa is reached during the pressure scan (see Fig. 5). At the other studied temperatures (308 K to 328 K) which are already above the critical temperature of CO_2 of 304 K, f_{fluid} varies smoothly with pressure as CO_2 transitions from the supercritical to the gaseous phase. For all cantilever lengths, the maximal slope of the dependence of f_{fluid} on the fluid pressure decreases with increasing CO_2 temperature, and its occurrence also shifts to higher values of CO_2 pressure (compare Figs. 6a–8a). This behavior is consistent with a lower sensitivity of the fluid density and viscosity to the fluid pressure above the critical temperature.

The evolution of the *Q*-factor with the fluid pressure also follows similar trends for all studied temperatures and cantilever lengths. Specifically, *Q*-factor decreases uniformly with the increasing fluid pressure due to the combined effect of the increasing fluid density and viscosity. While the variations of the *Q*-factor with pressure are rather small at high pressures, the *Q*-factor increases steeply at low pressures as the bandwidth of the frequency response gets narrower (see Figs. 5b–8b). For an ideal cantilever with zero internal losses, the vacuum value of *Q*-factor theoretically approaches infinity. In real cantilevers, however, internal damping causes finite *Q*-factor values observed at low fluid pressures. Maximal *Q*-factors observed in our measurements at the atmospheric pressure are ~80 at all studied temperatures. Analogical to the behavior of f_{fluid}, *Q*-factor of short cantilevers responds more sensitively to the fluid pressure, thus indicating again a greater sensing potential of such short cantilevers.

In Figs. 5–8, characteristics of the cantilever frequency response (f_{fluid} and *Q*-factor) at a given fluid temperature were plotted as functions of the fluid pressure. However, pressure and temperature do not enter directly into the hydrodynamic equations of motion of the immersed cantilever. Thus, the pressure-dependence plots provide only a limited insight into the mechanisms of the fluid–cantilever interaction. In contrast, fluid density is a natural control parameter that directly affects the cantilever resonant properties [6,13,20]. Furthermore, thermophysical properties of supercritical fluids (SCFs), such as viscosity and diffusivity, are governed mostly by the fluid density rather than the pressure. For example, the viscosity of CO_2 varies smoothly with density in the SCF region. We utilized the tables of the CO_2 density at varied CO_2 pressure and temperature from the NIST Chemistry WebBook [26] and plotted the values of f_{fluid} measured for cantilevers of a given length at all studied temperatures as a function of the CO_2 density. The results of this analysis are shown in Fig. 9 for the cantilevers with lengths of 225 μm (a) and 325 μm (b). From Fig. 9, it is evident that the values of f_{fluid} obtained for a fixed cantilever length at different fluid temperatures collapse on a single master curve over the range of densities that spans almost three orders of magnitude. Since f_{fluid} depends on both CO_2 density and viscosity, this observation implies that within the studied range of the CO_2 pressure and temperature, the CO_2 viscosity is a unique function of the CO_2 density. This remarkable behavior holds true not only in the supercritical phase of CO_2 but also in the region of the large density changes associated with the transition from gas to liquid.

In the following section, the relationship between the cantilever resonant characteristics ω_{fluid}, *Q*, and the density ρ and viscosity η of the immersion fluid is examined in detail. When analyzing oscillatory motion of a solid body with a characteristic size *w* in a viscous fluid, it is useful to introduce a nondimensional parameter characterizing the ratio of inertial and viscous forces acting on the body moving in the fluid—so-called Reynolds number $Re = (\rho\omega w^2)/(4\eta)$. According to the model of cantilever oscillations in the presence of fluid hydrodynamic forces developed by Sader [20], the frequency response of a weakly-damped cantilever can be described by Eq. (1), in which ω_{fluid} and *Q* depend on *Re*. In particular:

$$\omega_{fluid} = \frac{\omega_{vac}}{\sqrt{1 + \frac{\pi\rho w^2}{4\mu}\Gamma_r(Re)}}, \tag{3}$$

and

$$Q = \frac{\frac{4\mu}{\pi\rho w^2} + \Gamma_r(Re)}{\Gamma_i(Re)}. \tag{4}$$

In Eqs. (3) and (4), ω_{vac} is the vacuum resonant frequency of the cantilever, *w* is the cantilever width, μ is the cantilever mass per unit length, and Γ_r and Γ_i are the real and imaginary parts of the complex hydrodynamic function of the cantilever, respectively.

In the work of Sader [20], hydrodynamic function Γ was expressed as a combination of complex Bessel functions that did not provide a direct insight into the connection between the fluid parameters and the cantilever dynamics. Maali et al. introduced an analytical approximation to the hydrodynamic function Γ that is valid for the range of *Re* between 1 and 1000 and allows the derivation of closed formulas for the cantilever frequency response [21]. In this work, we operate in the range of $Re \sim [5; 100]$; for example, for a 325 μm long cantilever at 308 K and 7.58 MPa, the experimental values of $\rho = 286\ \mathrm{kg\,m^{-3}}$, $\omega = 2\pi \times 6500\ \mathrm{s^{-1}}$, $w = 20\ \mu\mathrm{m}$, and $\eta = 22.5\ \mu\mathrm{Pa\,s}$ give $Re \sim 52$. Hence, Maali's approximation is fully

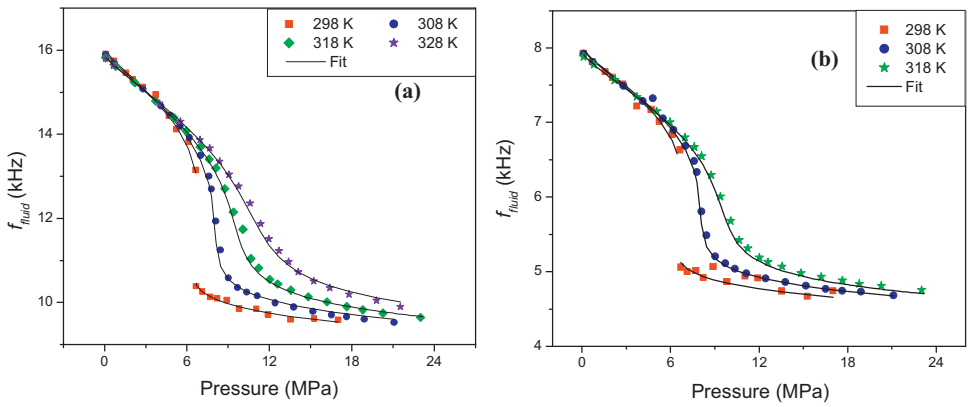

Fig. 10. Comparison of the experimental values of f_{fluid} (symbols) to the model of oscillations of a hydrodynamically damped cantilever (Eq. (7); solid lines) for (a) 225 μm and (b) 325 μm cantilevers at different CO_2 temperatures.

applicable to our experimental conditions. In Maali's notation, Γ_r can be expressed as

$$\Gamma_r(Re) = a_1 + \frac{a_2}{\sqrt{2Re}} = a_1 + a_2\sqrt{\frac{2\eta}{\rho\omega_{fluid}w^2}}, \quad (5)$$

and Γ_i reads as

$$\Gamma_i(Re) = \frac{b_1}{\sqrt{2Re}} + \frac{b_2}{2Re} = b_1\sqrt{\frac{2\eta}{\rho\omega_{fluid}w^2}} + b_2\frac{2\eta}{\rho\omega_{fluid}w^2}, \quad (6)$$

where $a_1 = 1.0553$, $a_2 = 3.7997$, $b_1 = 3.8018$, and $b_2 = 2.7364$ are empirical parameters determined by fitting the functional form of Eqs. (5) and (6) to the exact hydrodynamic function of Sader [21]. Upon inserting Eqs. (5) and (6) into Eqs. (3) and (4), we obtain

$$\omega_{fluid} = \omega_{vac}\left[1 + \frac{\pi\rho w}{4\rho_C t}\left(a_1 + a_2\sqrt{\frac{2\eta}{\rho\omega_{fluid}w^2}}\right)\right]^{-1/2} \quad (7)$$

and

$$Q = \frac{\frac{4\rho_C t}{\pi\rho w} + \left(a_1 + a_2\sqrt{\frac{2\eta}{\rho\omega_{fluid}w^2}}\right)}{b_1\sqrt{\frac{2\eta}{\rho\omega_{fluid}w^2}} + b_2\frac{2\eta}{\rho\omega_{fluid}w^2}}. \quad (8)$$

In Eqs. (7) and (8), we expressed the cantilever mass per unit length μ as the product of the cantilever density ρ_C, cantilever width w, and cantilever thickness t i.e. $\mu = \rho_C wt$. Expression identical to Eq. (7) was used in a recent study of Si cantilever oscillations in $scCO_2$ by Toda et al. [22].

Using the known cantilever width $w = 20$ μm and the values of ρ and η determined from the NIST Chemistry WebBook [26] for our experimental CO_2 pressures and temperatures, we fitted the self-consistent Eq. (7) to the experimental data points presented in Figs. 5a–8a that describe the dependence of f_{fluid} on the CO_2 pressure. The fitted parameters are the vacuum resonant frequency of the cantilever $\omega_{vac} = 2\pi f_{vac}$ and the product of the cantilever density and thickness $\rho_C t$ (we did not fit ρ_C and t separately as only their product enters into Eq. (7)). The results of fitting the experimentally obtained values of f_{fluid} to the predictions of Eq. (7) are summarized in Fig. 10 and Table 1. This figure and table illustrate a very good agreement between the model and the experiments. For all studied cantilever lengths and temperatures, the average relative error of the fit does not exceed 2.40% and the maximal relative error is less than 5.61%. From Table 1, it follows that the values of f_{vac} for 200 μm and 225 μm cantilevers decrease monotonously with increasing CO_2 temperature. For an elastic cantilever operating in the pure-bending regime, f_{vac} is given by [3]

$$f_{vac} = \frac{\kappa^2}{2\pi}\frac{1}{L^2}\sqrt{\frac{E\,t^2}{12\rho_C}} \quad (9)$$

where L is the cantilever length, E is the cantilever elastic modulus, and κ is a constant characterizing the cantilever oscillation mode ($\kappa = 1.875$ for the fundamental mode). In general, cantilever dimensions and elastic modulus change with temperature T and both these effects influence f_{vac}. Since the linear dimensions of the cantilever L, t grow as $\sim(1+\alpha\Delta T)$ and the cantilever density ρ_C decreases as $\sim(1+\alpha\Delta T)^{-3}$, the overall scaling of f_{vac} due to temperature-induced size changes is $f_{vac}(T+\Delta T) = f_{vac}(T)(1+\alpha\Delta T)^{0.5}$, where α is the coefficient of thermal expansion and ΔT is the temperature change. Similarly, E changes with temperature as $\sim(1+\beta\Delta T)$, where β is the coefficient of thermal dependence of the elastic modulus and, consequently, f_{vac} scales as $f_{vac}(T+\Delta T) = f_{vac}(T)(1+\beta\Delta T)^{0.5}$. For nickel, $\alpha = 1.3\times10^{-5}\,K^{-1}$ and β is between $-2\times10^{-4}\,K^{-1}$ and $-8\times10^{-4}\,K^{-1}$ [31]. Thus, the effect of the cantilever thermal expansion can be neglected in comparison to the temperature-induced changes of the cantilever elastic modulus. Experimental value of β can be then estimated from the measured f_{vac} obtained at different CO_2 temperatures. The average value of β calculated for 200 μm and 225 μm cantilevers from the data of Table 1 is $-7.2\times10^{-4}\,K^{-1}$ which agrees well with the literature data [31]. For 325 μm and 400 μm cantilevers, f_{vac} does not decrease with T when the CO_2 temperature increases from 298 K to 308 K. This departure from the observed trend is possibly caused by the high standard deviation of the measurements of f_{fluid} for the two longer cantilevers at 298 K which subsequently leads to a less precise determination of f_{vac} at 298 K. At higher temperatures, f_{vac} decreases with T also for 325 μm cantilever, at the same rate as for 200 μm and 225 μm cantilevers. The fitted product of the cantilever density and thickness, $\rho_C t$, is practically constant for all studied cantilever lengths and CO_2 temperatures; this is consistent with the procedure used for manufacturing the cantilevers (see Materials and methods section) and the weak dependence of the cantilever dimensions on temperature. A slight increase of the value of $\rho_C t$ with the cantilever length can likely be attributed to non-ideal clamping of the cantilevers at the support silicon base which displays a finite compliance and, thus, modifies the effective elastic bending modulus of the cantilever that enters into Eq. (9) [32].

Eq. (7) allows an estimation of the influence of the fluid viscosity on the resonant frequency, f_{fluid}, of an immersed cantilever for varied cantilever length. At a given density and viscosity of CO_2 (i.e. at a given temperature and pressure) and a constant cantilever width,

Table 1
Parameters f_{vac}, $\rho_C{}^*t$ determined from fitting the experimental data points of Figs. 5a–8a with Eq. (7) and the maximal and average relative errors between the experimental and predicted values of f_{fluid} and Q-factor for cantilevers of varying length at different CO_2 temperatures. Relative errors were calculated as differences between the corresponding measured and fitted values normalized by the fitted values.

Cantilever length (μm)	200			225				325			400	
temperature (K)	298	308	318	298	308	318	328	298	308	318	298	308
Vacuum resonant frequency, f_{vac} (kHz)	19.99	19.92	19.83	16.05	15.99	15.94	15.89	8.01	8.02	7.96	5.28	5.31
$\rho_C{}^*t$ (10^{-2} kg/m^2)	1.05	1.07	1.05	1.06	1.10	1.10	1.10	1.10	1.10	1.10	1.19	1.30
Maximal relative error f_{fluid} (%)	1.26	5.61	3.06	1.25	4.34	3.84	1.75	3.44	3.09	2.31	4.94	2.46
Average relative error f_{fluid} (%)	0.38	1.11	0.67	0.41	0.77	0.56	0.63	1.04	0.75	0.83	2.40	1.01
Average relative error Q (%)	11.95	10.08	6.18	12.81	8.18	8.41	7.72	14.42	9.98	10.56	40.33	47.54

the value of the variable second term in Eq. (5) for the real part of the cantilever hydrodynamic function Γ_r decreases with increasing f_{fluid} which is directly associated with smaller cantilever length. Thus, for shorter cantilevers, this variable term is less important with respect to the constant first term of Γ_r and can be neglected. Consequently, f_{fluid} given by Eq. (7) becomes approximately independent of the fluid viscosity and changes only due to the changing fluid density. This implies that with sufficiently short cantilevers, it should be possible to determine the fluid density from the measurement of f_{fluid} alone. However, if the cantilever length becomes comparable to its width, the assumption under which Eq. (7) was derived (cantilever length much larger than its width) no longer holds. Thus, cantilever length cannot be reduced deliberately in order to remove the coupling between f_{fluid} and the fluid viscosity.

According to Eq. (9), the vacuum resonant frequency, f_{vac}, should scale with the cantilever length, L, as $\sim 1/L^2$ at a constant temperature. In Fig. 11, we plotted the experimentally determined values of f_{vac} at 308 K as a function of $1/L^2$; temperature of 308 K was chosen because of the higher error of the estimates of f_{vac} at the lowest studied temperature of 298 K (see the discussion above). As illustrated by Fig. 11, f_{vac} is indeed linearly correlated with $1/L^2$ (coefficient $R^2 = 0.9999$), with a slope K_{exp} of 7.78×10^{-4} Hz m^2. This experimental value can be compared to the predicted K_{th} calculated from the Reuss model of a composite cantilever consisting of a nickel structural layer and a gold coating [33]:

$$K_{th} = \frac{\kappa^2}{2\pi}\sqrt{\frac{E_{Ni}t_{Ni}^2}{12\rho_{Ni}}(1+x)^2\sqrt{\frac{E_{Au}\rho_{Ni}}{(E_{Au}+xE_{Ni})(\rho_{Ni}+x\rho_{Au})}}}. \quad (10)$$

In the above expression, E_{Ni} is Young's modulus of nickel ($E_{Ni} = 200$ GPa), t_{Ni} is the thickness of the cantilever structural layer ($t_{Ni} = 900$ nm), ρ_{Ni} is the nickel density ($\rho_{Ni} = 8908$ kg m^{-3}), E_{Au} is Young's modulus of gold ($E_{Au} = 79$ GPa), t_{Au} is the thickness of the gold coating ($t_{Au} = 110$ nm), ρ_{Au} is the gold density ($\rho_{Au} = 19300$ kg m^{-3}), and $x = t_{Au}/t_{Ni}$. In Eq. (10), presence of an additional chromium layer on the cantilever was neglected as its thickness is much smaller than both t_{Ni} and t_{Au}. Upon inserting the material parameters and thicknesses of the nickel and gold layers into Eq. (10), we obtain $K_{th} \approx 6.75 \times 10^{-4}$ Hz m^2 which is smaller than the experimental value K_{exp} by ~13%. The relative deviation between K_{th} and K_{exp} is mostly caused by underestimation of the thickness of the nickel structural layer.

In order to compare the measured cantilever Q-factors to the predictions of the hydrodynamic damping model, we used Eq. (8) into which we inserted the values of the product $\rho_C t$ obtained previously from fitting of the experimental values of ω_{fluid} to Eq. (7) (data in Table 1) along with the values of ρ and η from the NIST Chemistry WebBook and measured ω_{fluid}. The results of this Q-factor comparison are provided in Fig. 12 and Table 1. As illustrated by Fig. 12, experimental Q-factors agree well with the predicted ones at higher CO_2 pressure where the Q-factor is low ($Q < 15$). The scatter in the data for Q-factors acquired in liquid CO_2 at the room temperature of 298 K without active temperature stabilization may be attributed to the ambient temperature fluctuations.

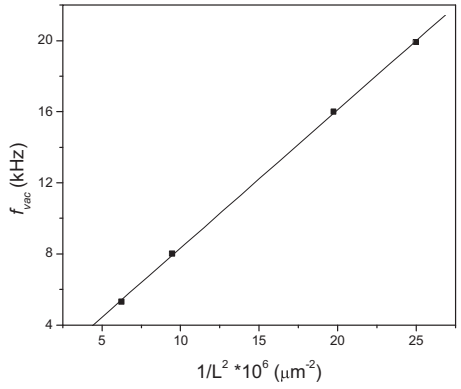

Fig. 11. Variation of f_{vac} with $1/L^2$ at 308 K. Squares represent experimental data points, solid line is the linear fit of the data.

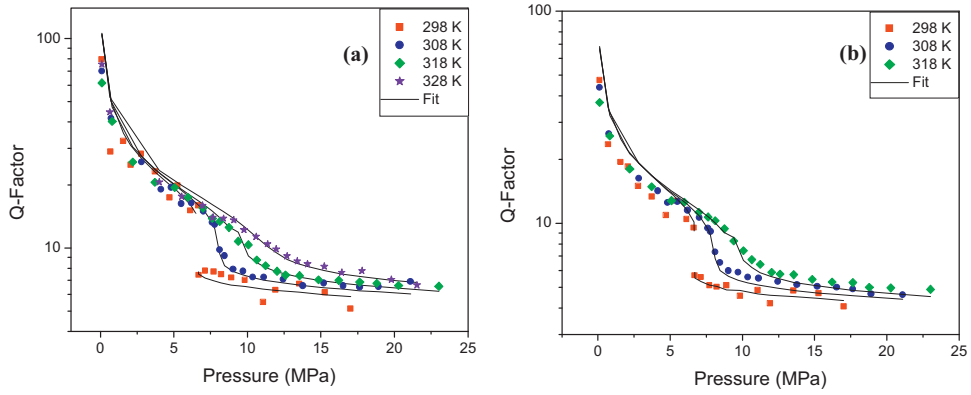

Fig. 12. Comparison of the experimental values of Q-factor (symbols) to the model of oscillations of a hydrodynamically damped cantilever (Eq. (8); solid lines) for (a) 225 μm and (b) 325 μm cantilevers at different CO_2 temperatures.

When the pressure decreases, the Q-factor increases and the difference between the measured and calculated Q-factors increases. As a result, the average errors of the Q-factor listed in Table 1 are about an order of magnitude higher than the corresponding errors of f_{fluid}. In order to understand this deviation, it is necessary to consider the various sources of cantilever damping that contribute to the overall observed Q-factor of the cantilever oscillations. For a cantilever immersed in a viscous fluid, the main source of damping lies in the shear forces acting in the fluid flowing around the cantilever; this is the damping described by Sader's model. Besides the viscous fluid damping, additional dissipation of the cantilever energy arises from internal friction in the cantilever material, energy loss to a compliant cantilever support, surface stresses, thermoelastic loss, and presence of additional material layers on the cantilever surface [34–37]. While the viscous damping dominates at high fluid pressure, relative importance of other damping sources increases at low fluid pressure corresponding to the decreasing fluid viscosity and density. All these additional damping mechanisms lower the overall Q-factor with respect to the value predicted solely by the hydrodynamic model, thus causing the departure of the measured Q-factors from the theoretical prediction. The dominant origin of the non-viscous damping in our experimental system is currently under investigation.

4. Conclusion

In this work, we carried out a systematic experimental study of the frequency response of microcantilevers of various sizes immersed in gaseous, liquid and supercritical CO_2. Our measurements were carried out with home-made magnetically actuated cantilevers immersed in CO_2 for which the pressure and temperature could be precisely controlled. We were able to acquire the characteristics of the cantilever oscillatory response (resonant frequency and Q-factor) under a wide range of CO_2 pressures and temperatures with high resolution and reproducibility. Subsequently, we analyzed our experimental data in the context of the model of cantilever oscillations under the influence of hydrodynamic forces proposed by Sader [20]. A very good agreement between our experimental results and model predictions confirms that Sader's approach is well applicable to the studies of microcantilever dynamic behavior in various fluid phases of CO_2.

Our study represents the first systematic attempt to the mapping of thermophysical properties of near-critical and supercritical fluids with the use of micromechanical resonators. Even though we concentrated on CO_2 as the model fluid, our experimental approach can be readily adopted to the measurement of the properties such as density and viscosity of other supercritical fluids including binary mixtures and to the detection of phase transitions in such mixtures (bubble and cloud points). Our technique can be possibly applied to investigate surface adsorption from supercritical solutions as well as catalytic reactions in supercritical fluids. The accessible range of the fluid temperatures and pressures can be extended by using different types of cantilevers and modified detection systems of the cantilever displacement.

Acknowledgement

We gratefully acknowledge Serhat Yavuz for his support in the fabrication of the microcantilevers.

References

[1] B. Ilic, D. Czaplewski, H.G. Craighead, P. Neuzil, C. Campagnolo, C. Batt, Mechanical resonant immunospecific biological detector, Applied Physics Letters 77 (2000) 450–452.
[2] G. Muralidharan, A. Wig, L.A. Pinnaduwage, D. Hedden, T. Thundat, R.T. Lareau, Absorption–desorption characteristics of explosive vapors investigated with microcantilevers, Ultramicroscopy 97 (2003) 433–439.
[3] K.M. Goeders, J.S. Colton, L.A. Bottomley, Microcantilevers, Sensing chemical interactions via mechanical motion, Chemical Reviews 108 (2008) 522–542.
[4] B. Rogers, L. Manning, M. Jones, T. Sulchek, K. Murray, B. Beneschott, J.D. Adams, Z. Hu, T. Thundat, H. Cavazos, S.C. Minne, Mercury vapor detection with a self-sensing, resonating piezoelectric cantilever, Review of Scientific Instruments 74 (2003) 4899–4901.
[5] A. Bongrain, C. Agnes, L. Rousseau, E. Scorsone, J.C. Arnault, S. Ruffinatto, F. Omnes, P. Mailley, G. Lissorgues, P. Bergonzo, High sensitivity of diamond resonant microcantilevers for direct detection in liquids as probed by molecular electrostatic surface interactions, Langmuir 27 (2011) 12226–12234.
[6] S. Boskovic, J.W.M. Chon, P. Mulvaney, J.E. Sader, Rheological measurements using microcantilevers, Journal of Rheology 46 (2002) 891–899.
[7] M. Youssry, N. Belmiloud, B. Caillard, C. Ayela, C. Pellet, I. Dufour, A straightforward determination of fluid viscosity and density using microcantilevers: from experimental data to analytical expressions, Sensors and Actuators A—Physical 172 (2011) 40–46.
[8] N. Belmiloud, I., Dufour, A., Colin, L. Nicu, Rheological behavior probed by vibrating microcantilevers, Applied Physics Letters 92 (2008), http://dx.doi.org/10.1063/1.2837181
[9] M. Hennemeyer, S. Burghardt, R.W. Stark, Cantilever micro-rheometer for the characterization of sugar solutions, Sensors 8 (2008) 10–22.
[10] A.R.H. Goodwin, E.P. Donzier, O. Vancauwenberghe, A.D. Fitt, K.A. Ronaldson, W.A. Wakeham, M.M. de Lara, F. Marty, B. Mercier, A vibrating edge supported plate, fabricated by the methods of micro electro mechanical system for the simultaneous measurement of density and viscosity: results for methylbenzene and octane at temperatures between (323 and 423) K and pressures in the range (0.1 to 68) MPa, Journal of Chemical Engineering Data 51 (2006) 190–208.
[11] P.I. Oden, G.Y. Chen, R.A. Steele, R.J. Warmack, T. Thundat, Viscous drag measurements utilizing microfabricated cantilevers, Applied Physics Letters 68 (1996) 3814–3816.
[12] M. Papi, G., Maulucci, G., Arcovito, P., Paoletti, M., Vassalli, M. De Spirito, Detection of microviscosity by using uncalibrated atomic force microscopy cantilevers, Applied Physics Letters 93 (2008), http://dx.doi.org/10.1063/1.2970963
[13] J.W.M. Chon, P. Mulvaney, J.E. Sader, Experimental validation of theoretical models for the frequency response of atomic force microscope cantilever beams immersed in fluids, Journal of Applied Physics 87 (2000) 3978–3988.
[14] A.M. Schilowitz, D.G. Yablon, E. Lansey, F.R. Zypman, Measuring hydrocarbon viscosity with oscillating microcantilevers, Measurement 41 (2008) 1169–1175.
[15] D.R. Franca, A. Blouin, All-optical measurement of in-plane and out-of-plane Young's modulus and Poisson's ratio in silicon wafers by means of vibration modes, Measurement Science and Technology 15 (2004) 859–868.
[16] A. Passian, R.J. Warmack, A. Wig, R.H. Farahi, F. Meriaudeau, T.L. Ferrell, T. Thundat, Observation of Knudsen effect with microcantilevers, Ultramicroscopy 97 (2003) 401–406.
[17] L.D. Landau, E.M. Lifshitz, Fluid Mechanics, Butterworth-Heineman, Oxford, 1998.
[18] N. McLoughlin, S.L., Lee, G. Hahner, Simultaneous determination of density and viscosity of liquids based on resonance curves of uncalibrated microcantilevers, Applied Physics Letters 89 (2006), http://dx.doi.org/10.1063/1.2374867
[19] H.L. Ma, J. Jimenez, R. Rajagopalan, Brownian fluctuation spectroscopy using atomic force microscopes, Langmuir 16 (2000) 2254–2261.
[20] J.E. Sader, Frequency response of cantilever beams immersed in viscous fluids with applications to the atomic force microscope, Journal of Applied Physics 84 (1998) 64–76.
[21] A. Maali, C. Hurth, R. Boisgard, C. Jai, T. Cohen-Bouhacina, J.P. Aime, Hydrodynamics of oscillating atomic force microscopy cantilevers in viscous fluids, Journal of Applied Physics 97 (2005), http://dx.doi.org/10.1063/1.1873060.
[22] M. Toda, T. Fujii, A. Yoshida, T. Hashida, T. Ono, Measurements of the phase transition and the average length of the density fluctuation under supercritical fluid using micromechanical resonators, Applied Physics Letters 99 (2011), http://dx.doi.org/10.1063/1.3610942.
[23] S.G. Kazarian, Polymer processing with supercritical fluids, Polymer Science Series C 42 (2000) 78–101.
[24] C.A. Barrett, A. Singh, J.A. Murphy, C. O'Sullivan, D.N. Buckley, K.M. Ryan, Complete synthesis of germanium nanocrystal encrusted carbon colloids in supercritical CO_2 and their superhydrophobic properties, Langmuir 27 (2011) 11166–11173.
[25] E.J. Beckman, Supercritical and near-critical CO_2 in green chemical synthesis and processing, Journal of Supercritical Fluids 28 (2004) 121–191.
[26] National Institute of Standards and Technology, Thermophysical properties of carbon dioxide, 2011. Available from: http://webbook.nist.gov/chemistry/fluid/
[27] A. Ozturk, H.I. Ocakli, N. Ozber, H. Urey, I.H. Kavakli, B.E. Alaca, A magnetically actuated resonant mass sensor with integrated optical readout, IEEE Photonics Technology Letters 20 (2008) 1905–1907.
[28] J.K. Luo, A.J. Flewitt, S.M. Spearing, N.A. Fleck, W.I. Milne, Young's modulus of electroplated Ni thin film for MEMS applications, Materials Letters 58 (2004) 2306–2309.

[29] A.L. Cohen, M.S., Lockard, K., Kim, Q.T., Le, G., Zhang, U., Frodis, D.S., Mcpherson, D.R. Smalley, US Patent 7 517 462, April 14, 2009.
[30] M.H. Bao, H. Yang, Squeeze film air damping in MEMS, Sensors and Actuators A—Physical 136 (2007) 3–27.
[31] J. Zacharias, The temperature dependence of Young's modulus for nickel, Physical Review 44 (1933) 116–122.
[32] L.A. Beardslee, A.M. Addous, K.S. Demirci, O. Brand, S.M. Heinrich, F. Josse, Geometrical optimization of resonant cantilevers vibrating in in-plane flexural modes, in: 2010 IEEE Sensors, IEEE, New York, 2010, pp. 1996–1999.
[33] J. Mertens, E. Finot, T. Thundat, A. Fabre, M.H. Nadal, V. Eyraud, E. Bourillot, Effects of temperature and pressure on microcantilever resonance response, Ultramicroscopy 97 (2003) 119–126.
[34] H. Hosaka, K. Itao, S. Kuroda, Damping characteristics of beam-shaped micro-oscillators, Sensors and Actuators A—Physical 49 (1995) 87–95.
[35] J.L. Yang, T. Ono, M. Esashi, Energy dissipation in submicrometer thick single-crystal silicon cantilevers, Journal of Microelectromechanical Systems 11 (2002) 775–783.
[36] A.R. Klempner, R.T. Marinis, P. Hefti, R.J. Pryputniewicz, Experimental determination of the Q-factors of microcantilevers coated with thin metal films, Strain 45 (2009) 295–300.
[37] T.J. Li, L. Bellon, Dissipation of micro-cantilevers as a function of air pressure and metallic coating, Europhysics Letters 98 (2012), http://iopscience.iop.org/0295-5075/98/1/14004/.